Restoring stiffness formulations and their influence on ship hydroelastic response

Conference Paper · October 2013

DOI: 10.1201/b15813-48

4 authors, including:

Neven Hadžić
University of Zagreb
40 PUBLICATIONS **52** CITATIONS
SEE PROFILE

Nikola Vladimir
University of Zagreb
112 PUBLICATIONS **213** CITATIONS
SEE PROFILE

Marko Tomic
University of Zagreb
41 PUBLICATIONS **124** CITATIONS
SEE PROFILE

Developments in Maritime Transportation and Exploitation of Sea Resources – Guedes Soares & López Peña (eds)
© 2014 Taylor & Francis Group, London, ISBN 978-1-138-00124-4

Restoring stiffness formulations and their influence on ship hydroelastic response

I. Senjanović, N. Hadžić, N. Vladimir & M. Tomić
University of Zagreb, Zagreb, Croatia

ABSTRACT: Hydroelastic analysis, with contemporary and well developed methodology, is capable of adequately capturing complex fluid-structure interaction related to ultra large container ships. A physical phenomenon of springing and whipping of modern container ships are commonly analyzed within hydroelastic methodology composed of three main parts, i.e. structural, hydrodynamic and hydrostatic mathematical model. In order to ensure valuable and reliable results, their proper definition is inevitable. This paper deals with three current restoring stiffness formulations, consistent one with distributed ship mass, consistent one with lumped masses and complete one. Consistent formulation is based on ship hydrostatics, while complete is structurally oriented with geometric stiffness included. Formulation of the restoring stiffness via the finite element method is developed as very useful approach for practical utilization of the hydroelasticity methodology. The validity of new developed approach is checked in a case of regular barge one real life container ship.

1 INTRODUCTION

The continuous growth of international maritime transport resulted in designing and building larger and faster container ships. As a result the first natural frequencies of such ships are quite low, especially in the case of large container ships due to open cross section and consequently reduced torsional stiffness (Bishop & Price 1979), and can easily fall into resonance with the encounter frequency in an ordinary sea spectrum (Pedersen 1985). Due to that fact traditional ship strength analysis, based on the assumption of ships as a rigid body, is not reliable enough (SNAME 1988). Therefore, it is necessary to perform the ship hydroelastic analysis, which can be defined as fluid-structure interaction type analysis relating external hydrodynamic and internal elastic forces.

Methodology of ship hydroelastic analysis, (Senjanović et al. 2007), includes definition of structural model with conventional stiffness, mass distribution, restoring stiffness, added mass, damping and wave excitation, and is based on the modal superposition method offering in such way a reduction of the number of equations and computing time (Malenica 2007).

The definition of restoring stiffness, as a part of the methodology of hydroelastic analysis, was found to be quite complex, (Senjanović et al. 2012a, Senjanović et al. 2013). The objective of this article is to investigate the impact of different restoring stiffness formulations on a hydroelastic response of real container ship structure in order to establish the required level of restoring stiffness complexity and to give recommendations for further practical usage. Three current formulations that are considered here are consistent formulation with distributed mass, (Senjanović et al. 2009), consistent formulation with lumped mass and complete restoring stiffness formulation, (Huang & Riggs 2000).

Recent advances in ship hydroelastic analysis cover a wide range of linear, nonlinear and impulsive quasi-static and dynamic response of both ship (Malenica & Derbanne 2012, Kim et al. 2012, Senjanović et al. 2012b) and floating structures (Meylan 2012).

2 INTEGRATION OF STIFFNESS COEFFICIENTS

Development of the current restoring stiffness formulations and their relationship are shown in Figure 1. Consistent restoring stiffness, Eq. (1) in Table 1, derived for ship structures, is based on variational principle and the method of virtual displacements (Senjanović et al. 2009).

Formulation (Huang & Riggs 2000), Eq. (2) in Table 1, called complete restoring stiffness, takes pressure change into account due to variation of depth and direction caused by structure deformation as well as the geometric stiffness based on still water stress distribution. The gravity term is

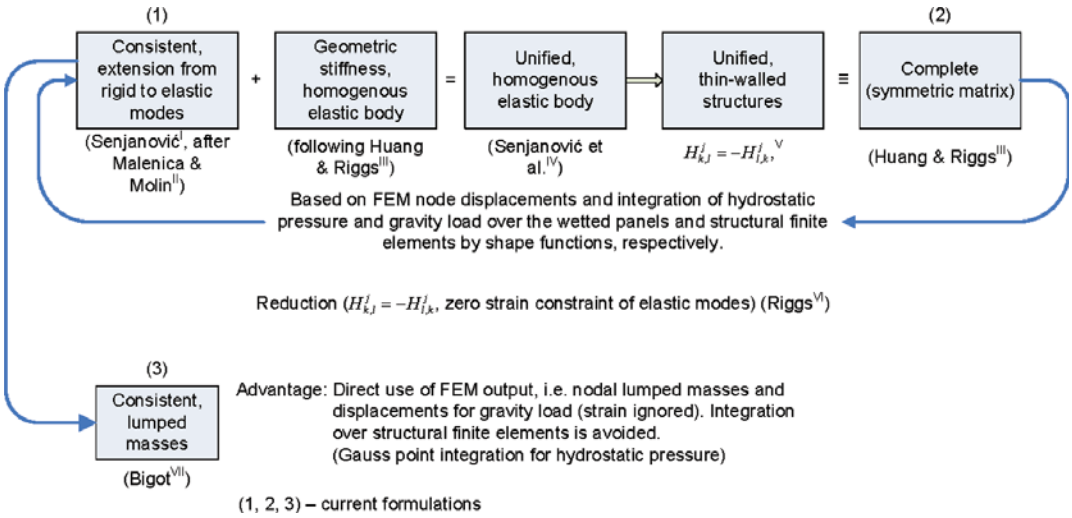

Figure 1. Current restoring stiffness formulations ([I]Senjanović et al. 2009, [II]Malenica et al. 2003, [III]Huang & Riggs 2000, [IV]Senjanović et al. 2011, [V]Senjanović et al. 2013, [VI]Riggs 2009, [VII]Bigot 2010).

Table 1. Current formulations of modal restoring stiffness.

Contribution from	Notation	Consistent*, Eq. (1)	Complete**, Eq. (2)	Unified***, Eq. (3)
a) Pressure	C^p_{ij}	$\rho g \iint_S H^i_k H^j_3 N_k \mathrm{d}S$	$\rho g \iint_S H^i_k H^j_3 N_k \mathrm{d}S$	$\rho g \iint_S H^i_k H^j_3 N_k \mathrm{d}S$
b) Normal vector and mode	C^{nh}_{ij}	$\rho g \iint_S Z H^i_k H^j_{l,l} N_k \mathrm{d}S$	$\rho g \iint_S Z H^i_k H^j_{l,l} N_k \mathrm{d}S$	$\rho g \iint_S Z H^i_k H^j_{l,l} N_k \mathrm{d}S$
c) Gravity load	C^m_{ij}	$g \iiint_V \rho_S H^i_k H^j_{3,k} \mathrm{d}V$		
d) Boundary stress (rigid body)	$-k^{S0}_{ij}$		$-\rho g \iint_S Z H^i_l H^j_{k,l} N_k \mathrm{d}S$	
e) Geometric stiffness	k^G_{ij}		$\iiint_V \Sigma_{kl} H^i_{m,k} H^j_{m,l} \mathrm{d}V$	$\iiint_V \Sigma_{kl} H^i_{m,k} H^j_{m,l} \mathrm{d}V$
f) Boundary stress (elastic body)	$-k^{SZ}_{ij}$			$\rho g \iint_S Z H^i_l H^j_{l,k} N_k \mathrm{d}S$
g) Structural deformation	$C^m_{ij} - k^{VZ}_{ij}$			$g \iiint_V \rho_S H^i_k \left(H^j_{3,k} + H^j_{k,3} \right) \mathrm{d}V$

*Senjanović et al 2009, **Huang & Riggs 2000, ***Senjanović et al 2011.

indirectly included as a rigid body part of geometric stiffness.

This formulation is suitable for general off-shore structures where geometric stiffness plays a dominant role and it results with symmetric restoring stiffness matrix. The Huang and Riggs formula can be transformed and reduced to the form of Eq. (1) in Table 1, (Riggs 2009).

The third formulation of restoring stiffness, Eq. (3) in Table 1, is obtained by unifying the consistent restoring stiffness, Eq. (1), and geometric stiffness, Eq. (2e), since they have some common terms, (Senjanović et al. 2011). As a result term $-k^{SZ}_{ij}$, Eq. (3f), occurs instead of $-k^{S0}_{ij}$, Eq. (2d), and also new term $C^m_{ij} - k^{VZ}_{ij}$, Eq. (3 g), appears. It was found in (Senjanović et al. 2013) that unified restoring stiffness is not applicable in the case of thin-walled structures, since mode derivatives $H^j_{l,k}$ and $H^j_{3,k}$ are not completely available in that case, Figure 2.

Integration of stiffness coefficients over the panels of the wetted surface can be performed either using the structural or the coarse hydrodynamic mesh, normally applied in the hydrodynamic analysis procedure. The latter is preferred due to computing time reduction but some difficulties arise since it is necessary to interpolate modal displacements from structural nodes to the new panel nodes and to approximately determine the corresponding modal derivatives, (Malenica et al. 2008). This is especially pronounced in the case of geometric stiffness, where the stress ten-

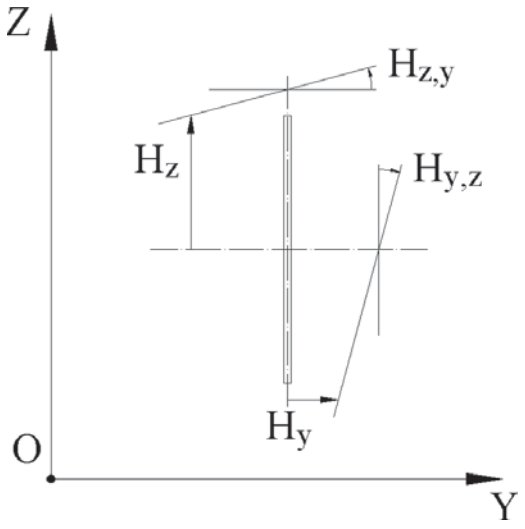

Figure 2. Relation between mode derivatives.

sor Σ_{kl} in global coordinate system is not known explicitly.

In order to perform a more reliable and accurate numerical integration of the surface and volumetric stiffness coefficients it is necessary to transform all involved quantities from the global to local coordinate system, and use shape functions for their distribution within the structural finite elements mesh, (Zienkiewicz 1971).

2.1 *Pressure coefficient*

The pressure coefficient expressed in index notation can be presented in matrix notation as

$$C_{ij}^{p} = \rho g \iint_{S} \left\langle N_x \; N_y \; N_z \right\rangle \begin{Bmatrix} H_x^i \\ H_y^i \\ H_z^i \end{Bmatrix} H_z^j \, \mathrm{d}S \tag{1}$$

By applying the well known finite element relations using transformation matrix, (A2), and shape functions, (Zienkiewicz 1971), after some rearrangement the pressure coefficient can be expressed as

$$C_{ij}^{p} = \rho g \left\langle N_x \; N_y \; N_z \right\rangle \sum_{k=1}^{M} \sum_{l=1}^{M} \begin{Bmatrix} H_{x,k}^i \\ H_{y,k}^i \\ H_{z,k}^i \end{Bmatrix} H_{z,l}^j \iint_{S} \phi_k \phi_l \, \mathrm{d}S \tag{2}$$

where k and l are nodal indices. The shape functions, ϕ_k and ϕ_l, are defined in the local coordinate system and can be integrated analytically for simple panels or numerically by Gauss points (Zienkiewicz 1971). All the other quantities in (5) are related to the global coordinate system.

2.2 *Normal vector and mode coefficient*

This coefficient can be presented in matrix notation as follows

$$C_{ij}^{nh} = \rho g \iint_{S} Z \left\langle N_x \; N_y \; N_z \right\rangle \begin{Bmatrix} H_x^i \\ H_y^i \\ H_z^i \end{Bmatrix} \times \left\langle \frac{\partial}{\partial X}, \frac{\partial}{\partial Y} \frac{\partial}{\partial Z} \right\rangle \begin{Bmatrix} H_x^j \\ H_y^j \\ H_z^j \end{Bmatrix} \mathrm{d}S. \tag{3}$$

By taking into account basic finite element relations, the shape functions can be grouped in the integrand

$$C_{ij}^{nh} = \rho g \left\langle N_x \; N_y \; N_z \right\rangle \sum_{k=1}^{M} \sum_{l=1}^{M} \begin{Bmatrix} H_{x,k}^i \\ H_{y,k}^i \\ H_{z,k}^i \end{Bmatrix} \times \left\langle H_{x,l}^j \; H_{y,l}^j \; H_{z,l}^j \right\rangle [c]^{\mathrm{T}} \iint_{S} Z \phi_k \begin{Bmatrix} \dfrac{\partial \phi_l}{\partial x} \\ \dfrac{\partial \phi_l}{\partial y} \\ \dfrac{\partial \phi_l}{\partial z} \end{Bmatrix} \mathrm{d}S. \tag{4}$$

2.3 *Boundary stress coefficient*

This coefficient written in matrix notation reads

$$-k_{ij}^{S0} = -\rho g \iint_{S} Z \left\langle H_x^i \; H_y^i \; H_z^i \right\rangle \begin{Bmatrix} \dfrac{\partial}{\partial X} \\ \dfrac{\partial}{\partial Y} \\ \dfrac{\partial}{\partial Z} \end{Bmatrix} \times \left\langle H_x^j \; H_y^j \; H_z^j \right\rangle \begin{Bmatrix} N_x \\ N_y \\ N_z \end{Bmatrix} \mathrm{d}S. \tag{5}$$

By taking into account finite element relations, and after some rearrangement one finds

$$-k_{ij}^{S0} = -\rho g \left\langle N_x \; N_y \; N_z \right\rangle \sum_{k=1}^{M}\sum_{l=1}^{M} \begin{Bmatrix} H_{x,l}^{j} \\ H_{y,l}^{j} \\ H_{z,l}^{j} \end{Bmatrix} \times \left\langle H_{x,k}^{i} \; H_{y,k}^{i} \; H_{z,k}^{i} \right\rangle [c]^{\mathrm{T}} \iint_S Z\phi_k \begin{Bmatrix} \dfrac{\partial \phi_l}{\partial x} \\ \dfrac{\partial \phi_l}{\partial y} \\ \dfrac{\partial \phi_l}{\partial z} \end{Bmatrix} \mathrm{d}S. \tag{6}$$

2.4 *Coefficient of gravity load—distributed mass*

The ship structure is modeled with shell finite elements of thickness h, so the volume integral in Eq. (1c) is reduced to the surface one, which can be written in matrix notation

$$C_{ij}^{m} = g\rho_S h \iint_S \left\langle H_x^i \; H_y^i \; H_z^i \right\rangle \begin{Bmatrix} \dfrac{\partial}{\partial X} \\ \dfrac{\partial}{\partial Y} \\ \dfrac{\partial}{\partial Z} \end{Bmatrix} H_z^j \, \mathrm{d}S. \tag{7}$$

If the mode displacements are expressed by nodal displacements and shape functions, (Zienkiewicz 1971), one obtains

$$C_{ij}^{m} = \rho_S g h \sum_{k=1}^{M}\sum_{l=1}^{M} \left\langle H_{x,k}^{i} \; H_{y,k}^{i} \; H_{z,k}^{i} \right\rangle H_{z,l}^{j} [c]^{\mathrm{T}} \times \iint_S \phi_k \begin{Bmatrix} \dfrac{\partial \phi_l}{\partial x} \\ \dfrac{\partial \phi_l}{\partial y} \\ \dfrac{\partial \phi_l}{\partial z} \end{Bmatrix} \mathrm{d}S. \tag{8}$$

2.5 *Coefficient of gravity load—lumped mass*

Concentrated mass elements are commonly used for modeling of ship cargo and equipment and they have to be taken into account within the volumetric integral of gravity load coefficient. Eq. (1c) expressed in expanded form, (Bigot 2010),

$$C_{ij}^{m} = gm \left(H_x^i \frac{\partial H_z^j}{\partial X} + H_y^i \frac{\partial H_z^j}{\partial Y} + H_z^i \frac{\partial H_z^j}{\partial Z} \right), \tag{9}$$

takes into account modal displacements, rotations and strain. By neglecting strain deformation terms and taking into account only the rotation component coefficient of gravity load for lumped mass can be expressed as

$$C_{ij}^{m} = gm \left[H_x^i \frac{1}{2}\left(-\alpha_y - \beta_y\right) + H_y^i \frac{1}{2}\left(\alpha_x + \beta_x\right) \right], \tag{10}$$

where α_x, α_y, β_x and β_y are angles of rotation about x and y axis respectively, Figure 3.

2.6 *Geometric stiffness*

Geometric stiffness, as well as the other restoring stiffness coefficients, represents energy which does not depend on the chosen coordinate system. Hence, the local coordinate system is used in this case due to easier derivation of geometric stiffness of finite element. The corresponding equation (2e) for an element written in matrix notation in the local coordinate system notation takes the form

$$k_{ij}^{G} = h \sum_{m} \iint_S \left\langle h_{m,k}^{i} \right\rangle [\sigma_{kl}] \left\{ h_{m,l}^{j} \right\} \mathrm{d}S, \tag{11}$$

where σ_{kl} are elements of stress matrix due to preloading in calm sea and m indicates mode components in x, y and z direction. After some rearrangement by applying finite element and well known mathematical relations, (Senjanović et al 2013, Zienkiewic 1971, Senjanović et al 2010), geometric stiffness coefficient takes the final form

$$k_{ij}^{G} = h \sum_{k=1}^{M}\sum_{l=1}^{M} \left(\langle c \rangle_x \left[H_{kl}^{ij} \right] \{c\}_x + \langle c \rangle_y \left[H_{kl}^{ij} \right] \{c\}_y + \langle c \rangle_z \left[H_{kl}^{ij} \right] \{c\}_z \right) \cdot \left(I_{11}^{kl}\sigma_{xx} + I_{21}^{kl}\sigma_{yx} + I_{12}^{kl}\sigma_{xy} + I_{22}^{kl}\sigma_{yy} \right), \tag{12}$$

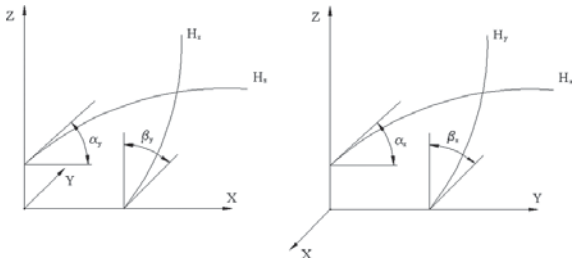

Figure 3. Angles of rotation about x and y axis.

where

$$I_{11}^{kl} = \iint_S \frac{\partial \phi_k}{\partial x}\frac{\partial \phi_l}{\partial x}\mathrm{d}S,\ I_{21}^{kl} = \iint_S \frac{\partial \phi_k}{\partial y}\frac{\partial \phi_l}{\partial x}\mathrm{d}S,$$
$$I_{12}^{kl} = \iint_S \frac{\partial \phi_k}{\partial x}\frac{\partial \phi_l}{\partial y}\mathrm{d}S,\ I_{22}^{kl} = \iint_S \frac{\partial \phi_k}{\partial y}\frac{\partial \phi_l}{\partial y}\mathrm{d}S. \quad (13)$$

If the local coordinate system coincides with the global one directional coefficients, expression (12), is reduced to the simpler form

$$k_{ij}^G = h\sum_{k=1}^{M}\sum_{l=1}^{M}\left(H_{x,k}^i H_{x,l}^j + H_{y,k}^i H_{y,l}^j + H_{z,k}^i H_{z,l}^j\right) \times\left(I_{11}^{kl}\sigma_{xx} + I_{21}^{kl}\sigma_{yx} + I_{12}^{kl}\sigma_{xy} + I_{22}^{kl}\sigma_{yy}\right) \quad (14)$$

Three terms exist in the first bracket and if one considers a finite element in xy plane, then the first two terms include membrane (in plane) displacements in x and y direction, while the third term is related to the element deflection in z direction. Hence, the third term is related to the ordinary geometric stiffness used in stability analysis, and therefore alone is not sufficient for hydroelastic analysis, (Senjanović et al 2013, Bigot 2010). The formulation of all derived coefficients for the case of three node triangular, four node rectangular and two node beam elements is given in (Senjanović et al 2013), respectively.

3 COMPUTER PROGRAM

The program is worked out for the ship hydroelastic analysis which is based on the modal superposition method, in order to reduce the number of differential equations of motion of the discretized structure and wetted surface. The dry natural modes of ship structure are used and they are determined by solving the eigenvalue problem formulated by the finite element method

$$\left(\left[K\right] - \Omega^2\left[M\right]\right)\left\{H\right\} = \left\{0\right\}, \quad (15)$$

where $[K]$ is the stiffness matrix, $[M]$ is the mass matrix, $\{H\}$ is a mode vector and Ω is a dry natural frequency.

The time domain differential equation of motion is derived in e.g. (Bishop & Price 1979) and due to consistency we only bring the modal differential equation of ship hydroelastic analysis in frequency domain which reads

$$\left\{\left(\left[k\right]+\left[C\right]\right) - i\omega\left(\left[d\right]+\left[B(\omega)\right]\right) - \omega^2\left(\left[m\right]+\left[A(\omega)\right]\right)\right\}\left\{\zeta\right\} = \left\{F(\omega)\right\}, \quad (16)$$

where $[k]$ is structural stiffness matrix, $[d]$ structural damping matrix, $[m]$ structural mass matrix, $[C]$ restoring stiffness matrix, $[B(\omega)]$ hydrodynamic damping matrix, $[A(\omega)]$ added mass matrix, $\{\xi\}$ modal amplitude vector, $\{F\}$ wave excitation vector and ω encounter frequency.

The integrated program for ship hydroelastic analysis consists of several modules.

NASTRAN, (MSC NASTRAN 2005), applied for 3D modeling of ship structure and calculation of dry natural vibrations, i.e. natural frequencies and modes, Eq. (18). This program is also used for ship strength calculation in calm water in order to determine the membrane stresses in geometric stiffness matrix. New developed software, RESTAN, is applied for the calculation of modal restoring stiffness. For determination of hydrodynamic coefficients, i.e. modal added mass, damping and wave excitation program HYDROSTAR, (HYDROSTAR 2006), is used and final modal ship motion equation (16) is solved using program MFRT.

Program RESTAN (REstoring STiffness ANalysis) is used for calculating the restoring stiffness coefficients according to the formulae worked out in the previous Section. Hence, there are two types of formulae; one set obtained by volume integration over the ship structure, and another over the wetted surface. For integration needs the necessary data generated by NASTRAN is used: node ordinary number and coordinates, ordinary number and nodes of the finite elements, material characteristics, components of modal displacements, stress components for ship in calm sea, etc. The wetted surface panels are taken from the 3D FEM model. Only wetted part of the panels intersected by the waterline is included in the wetted surface model. A logical scheme used for the generation of restoring stiffness matrix and performing the hydroelastic analysis is given in Figure 4.

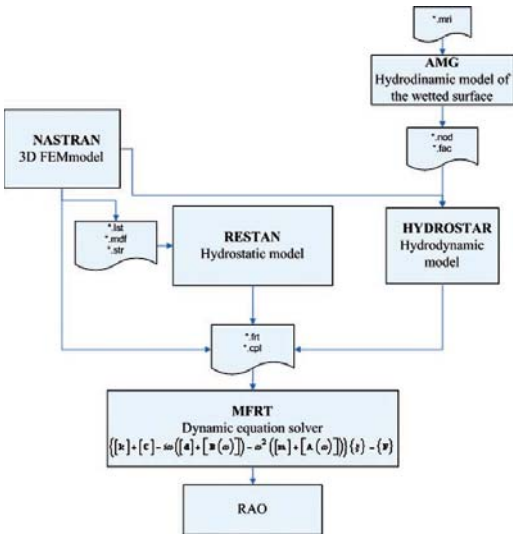

Figure 4. Logical scheme used for hydroelastic analysis.

4 TEST EXAMPLE

Application of the developed finite element formulation of restoring stiffness coefficients is tested in the case of a prismatic thin-walled barge, since in this case the restoring stiffness for rigid body modes can be determined analytically in order to verify the analysis procedure. The main particulars of the barge are the following:

Length	$L = 150$ m
Breadth	$B = 24$ m
Draught	$T = 6$ m
Depth	$D = 15$ m
Displacement	$\Delta = 22140$ t
Vertical position of center of gravity	$z_G = 7.5$ m
Waterplane area	$A_{WL} = 3600$ m^2
Water density	$\rho = 1.025$ t/m^3
Speed	$v = 0$ kn.

As shown in Figure 5, the inner barge structure consists of three longitudinal and 24 transverse bulkheads, and four decks. Thickness of all structural elements is 10 mm. The barge mass distribution is determined by specifying the density of the structural elements. In order to impose some vertical bending of the barge in calm sea, the density for elements in the aft and fore region of 36 m length is set to $\rho_1 = 0.260427$ t/m^3, while in the middle region of 78 m length the density is set to $\rho_2 = 0.781277$ t/m^3. The mass per unit length along the barge is shown in Figure 6.

The finite element mesh coincides with the topology of the barge structure in order to minimize local deformations vs girder ones. Longitudinal strength in calm water is performed by program NASTRAN. The barge still water sagging with the associated stress distribution is shown in Figure 7. The maximum stress occurs in the bottom and upper deck at the midship section, $\sigma_{\max} = \pm 137.5$ N/mm^2.

Structural damping used during the analysis is applied in a form of modal critical damping, ξ_{Di} (where i denostes mode number) according to the experience as follows

$$\begin{aligned}
&\xi_{D1} = \xi_{D2} = \xi_{D3} = \xi_{D5} = \xi_{D6} = 0,\\
&\xi_{D4} = 0.070, \xi_{D7} = 0.015, \xi_{D8} = 0.020,\\
&\xi_{D9} = 0.022, \xi_{D10} = 0.025, \xi_{D11} = 0.035,\\
&\xi_{D12} = 0.045, \xi_{D13} = 0.055, \xi_{D14} = 0.070,\\
&\xi_{D15} = 0.080, \xi_{D16+} = 0.100.
\end{aligned} \tag{17}$$

The free vibration calculation is also performed by NASTRAN for the same mass distribution as specified above. The natural frequencies of the first four vertical, horizontal and torsional modes are listed in Table 2.

The first one of each vibration types are shown in Figures 8, 9 and 10. No coupling between horizontal and torsional vibrations is encountered in this case, since the torsional and gravity centre are the same point.

Three numerical calculations of restoring stiffness are performed. The first one is for the con-

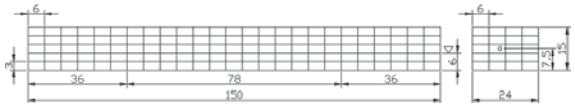

Figure 5. Thin-walled barge structure.

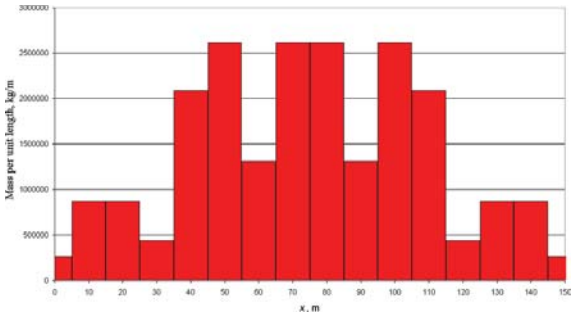

Figure 6. Thin-walled barge—mass per unit length, kg/m.

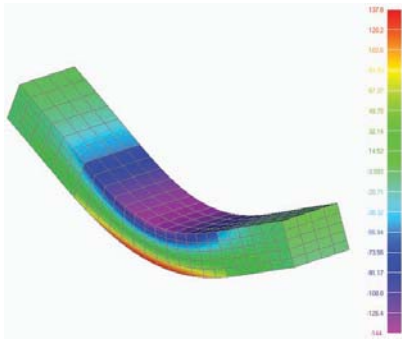

Figure 7. Stress distribution in calm sea, prismatic barge, N/mm^2.

Table 2. Dry natural frequencies of prismatic barge, Ω, [Hz].

Mode	Vertical	Horizontal	Torsional
1	1.4611	2.1674	2.9425
2	3.1266	4.5227	5.4358
3	5.3028	7.5194	7.4517
4	7.7376	10.8088	9.5297

sistent stiffness with distributed structural mass, Eq. (1). The second calculation is also performed for the consistent stiffness, but the gravity coefficient, C_{ij}^{m}, Eq. (1c), is determined by employing the fully lumped masses (without the rotational components). The third calculation deals with the complete restoring stiffness, Eq. (2). The calculated coefficients and the resulting stiffness are listed in Table 3. The following units are used in all calculations: N, m, s, kg.

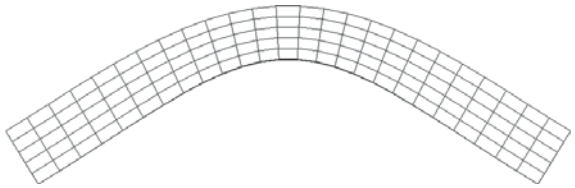

Figure 8. The first vertical mode, prismatic barge.

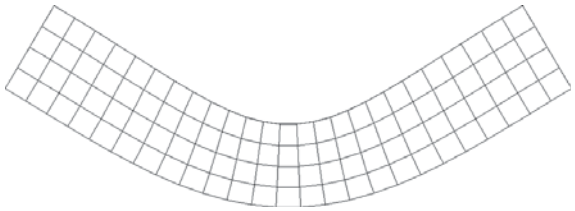

Figure 9. The first horizontal mode, prismatic barge.

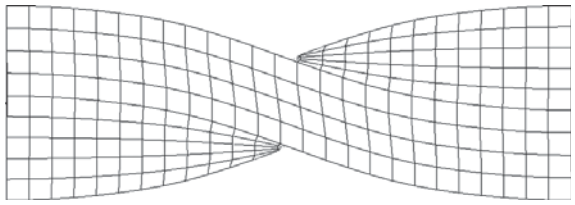

Figure 10. The first torsional mode, prismatic barge.

For heave only pressure coefficient C_{33}^{p} is relevant. Almost the exact value is obtained in all three calculations, $\varepsilon = 0.025\%$. For roll motion, the pressure coefficient C_{44}^{p} has the main contribution. Since reference point coincides with the centre of gravity coefficients C_{44}^{nh} and C_{44}^{m} are zero. The value of C_{44}^{tot} for roll is very close to the exact value, $\varepsilon = 0.01\%$. In the complete restoring stiffness it is obvious that $-k_{44}^{S0} + k_{44}^{G} \approx 0$ as it is expected since that expression has to compensate C_{44}^{m} which is equal to zero. Discrepancy of the total coefficient, $\varepsilon = 0.007\%$, is very small. Pitch restoring is not as sensitive as that of roll, so discrepancies in all three cases are considerably smaller.

Hydroelastic response of the considered barge was determined for the case of heading angle $\chi = 150°$ (following waves $\chi = 0°$). A large number of wave frequencies in the range from 0.1 to 1.5 rad/s, with step $\Delta\omega = 0.02$ rad/s is taken into account.

In the following figures transfer functions of sectional forces are shown. Moments are related to the midship section, while shear forces are determined at the aft section $0.25L$, where it is expected to have maximum values. The RAO of the vertical bending moment, Figure 11, achieves peak value at $\omega = 0.605$ rad/s. The response curves for all three restoring stiffness formulations are the same. RAO of vertical shear force, Figure 12, manifests peak at $\omega = 0.63$ rad/s. The response curves are very close to each other.

The RAO of horizontal bending moment is shown in Figure 13. The maximum peak occurs

Table 3. Restoring stiffness coefficients of prismatic barge, C.

Motion	Formulation	C_{ij}^{p}	C_{ij}^{nh}	C_{ij}^{m}	$-k_{ij}^{S0}$	k_{ij}^{G}	C_{ij}^{total}	C_{ij}^{an}	ε (%)
Heave $i=j=3$	Consistent dist. mass	$3.6199 \cdot 10^{7}$	0.0	0.0			$3.6199 \cdot 10^{7}$	$3.6190 \cdot 10^{7}$	0.025
	Consistent lumped mass	$3.6199 \cdot 10^{7}$	0.0				$3.6199 \cdot 10^{7}$		0.025
	Complete	$3.6199 \cdot 10^{7}$	0.0				$3.6199 \cdot 10^{7}$		0.025
Roll $i=j=4$	Consistent dist. mass	$7.6018 \cdot 10^{8}$	0.0	0.0			$7.6018 \cdot 10^{8}$	$7.601 \cdot 10^{8}$	0.010
	Consistent lumped mass	$7.6018 \cdot 10^{8}$	0.0						
	Complete	$7.6018 \cdot 10^{8}$	0.0		$2.2805 \cdot 10^{9}$	$-2.2806 \cdot 10^{9}$	$7.6015 \cdot 10^{8}$		0.007
Pitch $i=j=5$	Consistent dist. mass	$6.6896 \cdot 10^{10}$	0.0	0.0			$6.6896 \cdot 10^{10}$	$6.6890 \cdot 10^{10}$	0.009
	Consistent lumped mass	$6.6896 \cdot 10^{10}$	0.0						
	Complete	$6.6896 \cdot 10^{10}$	0.0		$2.2805 \cdot 10^{9}$	$-2.2806 \cdot 10^{9}$	$6.6896 \cdot 10^{10}$		0.009

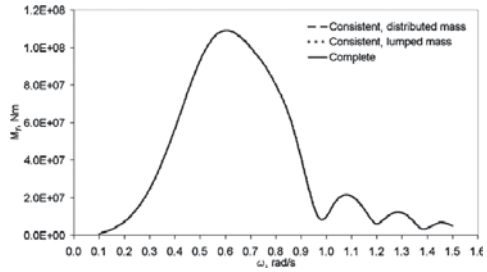

Figure 11. Transfer function of vertical bending moment at midship section, prismatic barge, $\chi = 150°$.

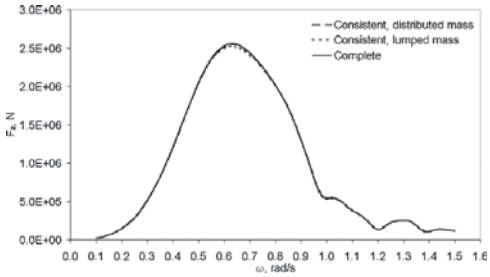

Figure 12. Transfer function of vertical shear force, prismatic barge, $\chi = 150°$, $x = 37.5$ m.

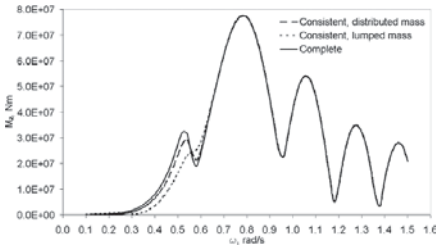

Figure 13. Transfer function of the horizontal bending moment at midship section, prismatic barge, $\chi = 150°$.

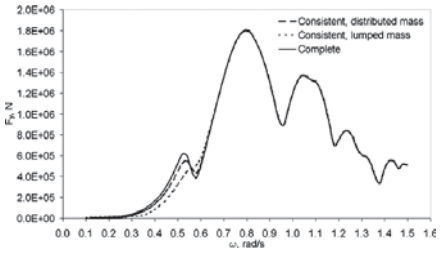

Figure 14. Transfer function of the horizontal shear force, prismatic barge, $\chi = 150°$, $x = 37.5$ m.

at $\omega = 0.78$ rad/s. There are some differences of the response curves at the first peak at $\omega = 0.52$ rad/s, while elsewhere in the frequency region the response is the same. That is similar for the RAO of the horizontal shear force, Figure 14. In ship

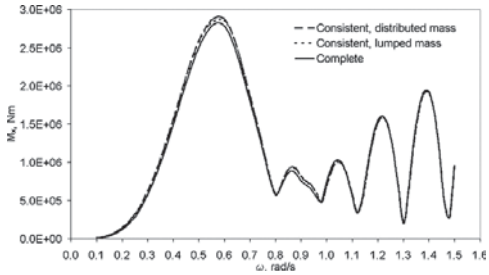

Figure 15. Transfer function of the torsional moment at midship section, prismatic barge, $\chi = 150°$.

Table 4. Prismatic barge—peak and resonance frequency for different restoring stiffness formulations.

Formulation	Peak, Nm	Resonance frequency shifting, rad/s
Vertical bending moment		
Consistent, distributed mass	$1.8877 \cdot 10^8$	0.605
Consistent, lumped mass	$1.0881 \cdot 10^8$	0.605
Complete	$1.0878 \cdot 10^8$	0.605
Torsional moment		
Consistent, distributed mass	$2.9111 \cdot 10^6$	0.575
Consistent, lumped mass	$2.8750 \cdot 10^6$	0.575
Complete	$2.8244 \cdot 10^6$	0.575
Horizontal bending moment (1st peak)		
Consistent, distributed mass	$2.8893 \cdot 10^7$	0.54
Consistent, lumped mass	/	/
Complete	$3.2208 \cdot 10^7$	0.52
Horizontal bending moment (2nd peak)		
Consistent, distributed mass	$7.7768 \cdot 10^7$	0.78
Consistent, lumped mass	$7.6728 \cdot 10^7$	0.78
Complete	$7.7582 \cdot 10^7$	0.78

hydroelastic analysis the most interesting RAO is that of torsional moment. In the considered case maximum value occurs at $\omega = 0.575$ rad/s, and response curves determined by different restoring stiffness formulations follow each other very well, Figure 15.

Some of the differences between peaks and resonance frequencies for each restoring stiffness formulation are given in Table 4 for the case of prismatic barge.

5 ILLUSTRATIVE EXAMPLE

Application of the developed finite element formulation of restoring stiffness coefficients is illus-

trated in a case of real container ship whose main particulars are the following:

Length over all	$L_{oa} = 349.00$ m
Length between perpendiculars	$L_{pp} = 333.44$ m
Breadth	$B = 42.80$ m
Draught	$T = 13.10$ m
Depth	$D = 27.30$ m
Displacement	$\Delta = 125604$ t
Water density	$\rho = 1.025$ t/m^3
Capacity	9415 TEU
Speed	$v = 25$ kn.

General arrangement of a 9415 TEU container ship is shown in Figure 16. 3D FEM model, consisting of 84893 elements and 16966 structural nodes, was generated in program NASTRAN with purpose of performing the ship still water strength and free vibration analysis. Container cargo was modeled using the concentrated mass elements rigidly connected with the surrounding structural nodes. In such a way sectional cargo mass is lumped in its center of gravity.

The ship hogging in calm sea with stress distribution is shown in Figure 17. Natural frequencies of the first six dry natural modes are listed in Table 5 while first two coupled horizontal and torsional and first vertical mode are shown in Figures 18 and 19 respectively.

Three numerical calculations of restoring stiffness are performed, as described in Section 5. Validation of the calculations can be checked in the case of heave, roll and pitch since the restoring stiffness for these three motions can be determined analytically using the well known seakeeping restoring stiffness expressions, (SNAME 1988). The calculated coefficients and the resulting stiffness are listed in Table 6. The following units are used in all calculations: N, m, s, kg.

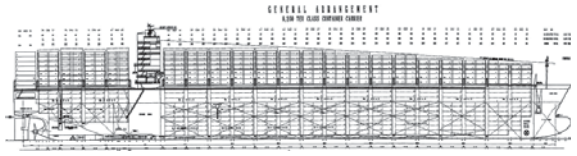

Figure 16. General arrangement of a 9415 TEU container ship.

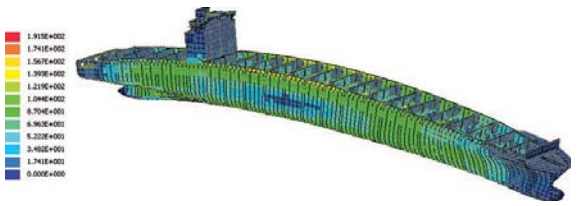

Figure 17. Von Mises stress distribution in calm sea, 9415 TEU container ship, N/mm^2.

Table 5. Natural frequencies of 9415 TEU container ship, Ω, [Hz].

Mode no.	Description	f_i, [Hz]
1	H1+T1	0.415
2	H1+T2	0.588
3	V1	0.676
4	H2+T3	1.018
5	V2	1.384
6	H3+T4	1.391

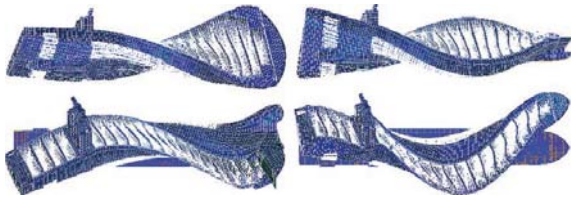

Figure 18. The first and the second coupled torsional and horizontal mode shapes (lateral and bird's view), 9415 TEU container ship.

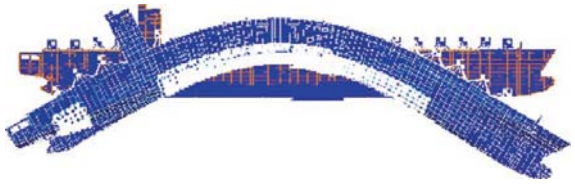

Figure 19. The first vertical mode, 9415 TEU container ship.

For heave only pressure coefficient C_{33}^{p} is relevant. Almost the exact value is obtained in all three calculations, $\varepsilon = 1.067\%$ for the fist and third formulation, and $\varepsilon = 0.638\%$ in the case of the second one.

Slightly larger disagreement between calculated and analytical value is obtained in the case of roll, i.e. $\varepsilon = -1.575\%$ for consistent and $\varepsilon = 1.457\%$ for consistent formulation with lumped masses. Special attention has to be given to the restoring stiffness coefficient in the case of complete formulation, since boundary stress coefficient, k_{44}^{S0}, and geometric stiffness coefficient, k_{44}^{G}, are two close values that cancel each other, (Senjanović et al. 2013), and in the case of ship structure they are for one order of magnitude greater than the pressure coefficient. Also, due to high complexity of

Table 6. Restoring stiffness coefficients of 9415 TEU container ship, *C*.

Motion	Formulation	C_{ij}^{p}	C_{ij}^{nh}	C_{ij}^{m}	$-k_{ij}^{S0}$	k_{ij}^{G}	C_{ij}^{total}	C_{ij}^{an}	ε (%)
Heave $i=j=3$	Consistent dist. mass	$1.2027\cdot10^{8}$					$1.2027\cdot10^{8}$	$1.1900\cdot10^{8}$	1.067
	Consistent lumped mass	$1.1976\cdot10^{8}$					$1.1976\cdot10^{8}$		0.638
	Complete	$1.2027\cdot10^{8}$					$1.2027\cdot10^{8}$		1.067
Roll $i=j=4$	Consistent dist. mass	$1.7209\cdot10^{9}$	$-3.9588\cdot10^{7}$	$-1.9863\cdot10^{7}$*			$1.6614\cdot10^{9}$	$1.6880\cdot10^{9}$	–1.575
	Consistent lumped mass	$1.7346\cdot10^{9}$	0.0	$-2.1990\cdot10^{7}$			$1.7126\cdot10^{9}$		1.457
Pitch	Complete	$1.7209\cdot10^{9}$	$-3.9588\cdot10^{7}$		$2.9021\cdot10^{10}$	$-2.9026\cdot10^{10}$*	$1.6820\cdot10^{9}$		–0.355
	Consistent	$8.3199\cdot10^{11}$	$1.3976\cdot10^{8}$	$2.7184\cdot10^{8}$			$8.3240\cdot10^{11}$	$8.2020\cdot10^{11}$	1.487

the geometric stiffness coefficient calculation and its dependence on the ship strength analysis it is not possible to achieve close values of those two coefficients, i.e. real value obtained in the case of roll is $k_{44}^{G}=-2.9902\cdot10^{10}$ that is only 3% larger comparing to the value of boundary stress coefficient. Therefore, even a small difference between those two coefficients causes significant error in the value of the total restoring coefficients and consequently making the complete formulation, although physically correct, numerically unstable. To enable adequate comparison of the achieved results the final value of the geometric stiffness coefficient in the case of complete formulation was calibrated with respect to roll in order to cancel the contribution of the boundary stress coefficient.

Except that, special care has to be taken in the case of gravity coefficient, C_{44}^{m}. It can easily be shown that in the case of rigid body modes and when the centre of gravity is taken as the reference point, Eq. (1c) yields zero value. This condition is easily achieved in the case of simpler structures like prismatic barge, (Senjanović et al. 2013), and it is also approximately satisfied in the case of complex structure with continuous or lumped mass. Some problems arise with combined continuous and lumped mass approach making the gravity coefficient very sensitive to mass modeling.

Due to that fact the value of gravity coefficient was also calibrated by correcting the vertical position of the center of gravity of the chosen concentrated cargo. In such way, the original value of $C_{44}^{m}=-1.714\cdot10^{8}$ was reduced to $C_{44}^{m}=-1.9863\cdot10^{7}$, which is negligible, comparing to the value of pressure coefficient, $C_{44}^{p}=1.7209\cdot10^{9}$, Table 6. Restoring stiffness in the case of pitch is not as sensitive as in the case of roll, and all the achieved values are close to the analytical ones.

Hydroelastic response of the considered container ship was determined for the case of heading angle $\chi=150°$ (following waves $\chi=0°$) and for the same range of frequencies as in the case of regular barge. Moments are related to the midship section, while shear forces are determined at the aft section 0.25 *L*, where it is expected to have maximum values. RAO of the vertical bending moment, Figure 20, achieves significant peak value at $\omega=0.72$ rad/s.

The response curves for all three restoring stiffness formulations are the same. RAO of vertical shear force, Figure 21, manifests the first peak at $\omega=0.78$ rad/s. The response curves are very close to each other. RAO of horizontal bending moment is shown in Figure 22. The significant peak occurs at $\omega=0.91$ rad/s with good agreement between all formulations. That is similar for the RAO of the horizontal shear force, Figure 23. In the case of torsional moment RAO, Figure 24, the first signifi-

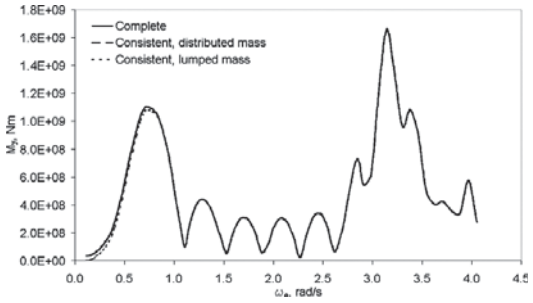

Figure 20. Transfer function of vertical bending moment at midship section, 9415 TEU container ship, $\chi = 150°$.

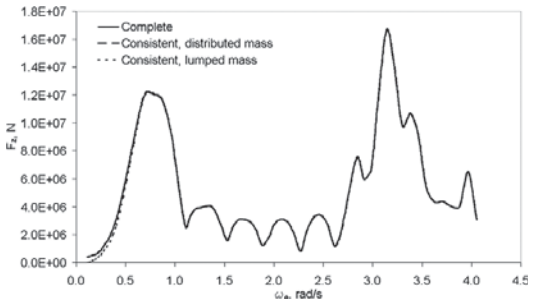

Figure 21. Transfer function of vertical shear force, 9415 container ship, $\chi = 150°$, $x = 85$ m.

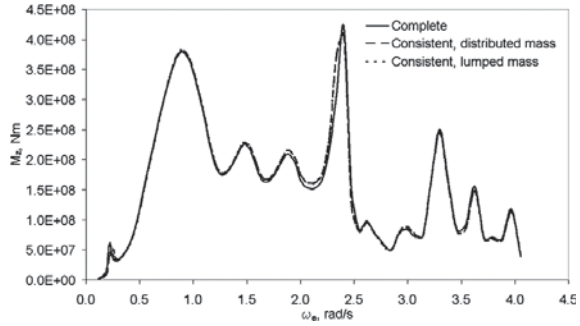

Figure 22. Transfer function of horizontal bending moment at midship section, 9415 TEU container ship, $\chi = 150°$.

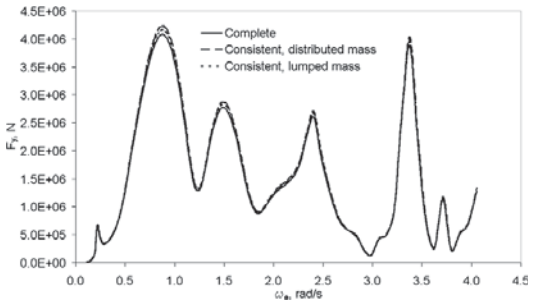

Figure 23. Transfer function of horizontal shear force, 9415 TEU container ship, $\chi = 150°$, $x = 85$ m.

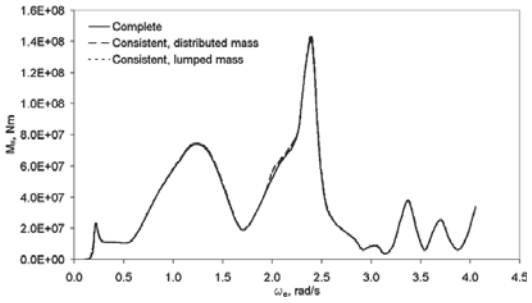

Figure 24. Transfer function of torsional moment at midship section, 9415 TEU container ship, $\chi = 150°$.

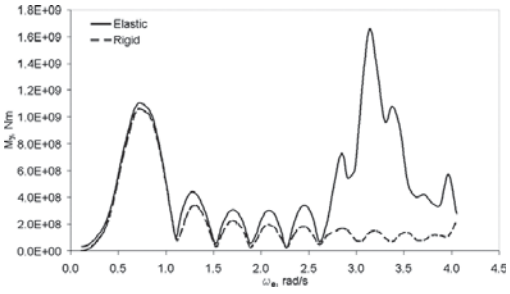

Figure 25. Transfer function of vertical bending moment for rigid and elastic ship at midship section, $\chi = 150°$.

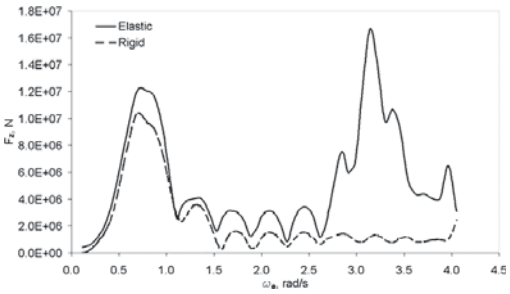

Figure 26. Transfer function of vertical shear force for rigid and elastic ship, $\chi = 150°$, $x = 85$ m.

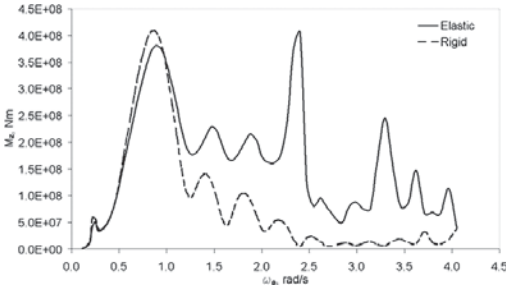

Figure 27. Transfer function of horizontal bending moment for rigid and elastic ship at midship section, $\chi = 150°$.

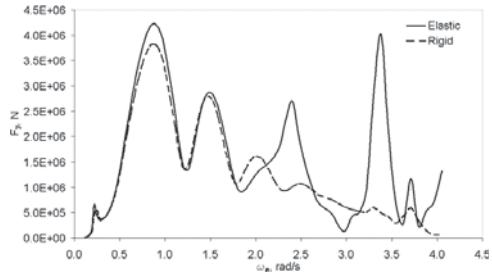

Figure 28. Transfer function of horizontal shear force for rigid and elastic ship, $\chi = 150°$, $x = 35$ m.

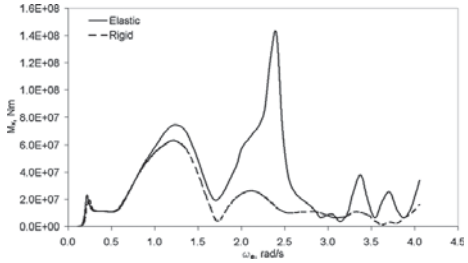

Figure 29. Transfer function of torsional moment for rigid and elastic ship at midship section, $\chi = 150°$.

cant peak occurs at $\omega = 1.25$ rad/s, and response curves determined by different restoring stiffness formulations follow each other very well.

In Figures 25 to 29 transfer functions of sectional forces determined by the ordinary procedure for rigid body motion and hydroelastic analysis with consistent restoring stiffness and distributed mass are shown. Rigid body values at resonant motions are somewhat lower than those of the elastic body. Resonances of elastic response are captured in the area of higher encounter frequencies where the ordinary procedure based on a ship as rigid body is not applicable.

6 CONCLUSIONS

Theoretical improvement and formulation of the restoring stiffness via finite element method, that is very useful for practical utilization because it enables the usage of 3D FEM model as integration domain within the hydrostatic model, are presented. The validity of the numerical procedure was demonstrated in the case of prismatic barge with very good agreement between numerical and available analytical values.

Restoring stiffness of ship structure was determined by program RESTAN using the modal displacements and stress distribution determined via commercial program NASTRAN. Total geometric stiffness was also determined by program RESTAN which comprises three parts related to both translatory and membrane displacements. The effect on the hydroelastic response was examined for three restoring stiffness formulations: consistent with distributed mass, consistent with lumped masses and complete one. A good agreement was found between all results of three formulations. Also, good agreement of the results was achieved in the case of rigid body modes where numerical and analytical values exist. The only exception is numerical instability of complete formulation in the case of roll.

Finally, it can be concluded that the restoring stiffness analysis using complete formulation is, although physically correct, very complex and extensive and does not result with expected accuracy improvement. Due to that fact this formulation is not suitable for the practical usage in shipping industry. On the other hand, consistent formulation with lumped mass is much simpler and gives very good results. Therefore it can be recommended for the further utilization.

REFERENCES

Bigot, F. 2010. WP4: Global hydro elastic loading & responses—D4.3: Interface module for coupling 3D FEM structural model to 3D hydrodynamic model', FP7 TULCS project, Bureau Veritas, Paris.

Bishop, R.E.D. & Price, W. G. 1979. *Hydroelasticity of Ships*. Cambridge University Press.

Huang, L.L. & Riggs, H.R. 2000. The hydrostatic stiffness of flexible floating structures for linear hydroelasticity, Marine Structures,13, pp. 91–106.

HYDROSTAR 2006. User's Manual, Bureau Veritas, Paris.

Kim, J.H et al. 2012. Analysis on Ship Springing Using Fully—Coupled FSI Models. *Hydroelasticity in Marine Technology*, Tokyo, Japan., pp. 95–105.

Malenica, Š. et al. 2003. Hydroelastic response of a barge to impulsive and non—impulsive wave loads. *Hydroelasticity in Marine Technology*, Oxford, U.K., pp. 107–115.

Malenica, Š. 2007. Hydro-structure interactions in seakeeping. In: Terze, Z., Lacor, Ch. (Eds.), Proceedings of the International Workshop on Coupled Methods in Numerical Dynamics CMWD, pp. 231–256.

Malenica, Š. et al. 2008. Some aspects of 3D linear hydroelastic models of springing. *Internantional Conference on Hydrodynamics*, Nantes. 2008.

Malenica, Š. & Derbanne, Q. 2012. Hydro-Elastic issues in the Design of Ultra Large Container Ships—TULCS Project. *Hydroelasticity in Marine Technology*, Tokyo, Japan., pp. 223–247.

Meylan, M.H. 2012. The Linear Transient Response of a Hydroelastic body and Its Approximation Using the Singularity Expansion Method. *Hydroelasticity in Marine Technology*, Tokyo, Japan., pp. 439–445.

MSC. NASTRAN 2005, Installation and Operation Guide, MSC. Software.

Pedersen, P. T. 1985. Torsional response of containerships. *Journal of Ship Research*, 29 (3), pp. 194–205.

Riggs, H. R. 2009. Comparison of formulations for the hydrostatic stiffness of flexible structures, *ASME Journal of Offshore Mechanics and Arctic Engineering*, Vol 131/024501.Senjanović, I. et al. 2007. Methodology of ship hydroelasticity investigation. *Brodogradnja,* 58–2, pp. 133–145.

Senjanović, I. et al. 2009. Hydroelasticity of large container ships, *Marine Structures* 22, pp. 287–314.

Senjanović, I. et al. 2010. Some aspects of geometric stiffness modeling in hydroelastic analysis of ship structures. *Transactions of FAMENA* XXXIV—4.

Senjanović, I. et al. 2011. Investigation of restoring stiffness in the hydroelastic analysis of slender marine structures. *ASME Journal of Offshore Mechanics and Arctic Engineering*, Vol 133/031107-1.

Senjanović, I. et al. 2012a. Formulation of consistent restoring stiffnes in ship hydroelastic analysis. *Journal of Engineering Mathematics* 72, pp. 141–157.

Senjanović, I. et al. 2012b. Improved Methodology of Ship Hydroelastic Analysis. *Hydroelasticity in Marine Technology*, Tokyo, Japan., pp. 115–125.

Senjanović, I. et al. 2013. Finite element formulation of different restoring stiffness issues in the ship hydroelastic analysis and their influence on response. *Ocean Engineering*.

SNAME, 1988. *Principles of Naval Architecture*. Jersey City, SNAME.

Zienkiewicz, O.C. 1971. The Finite Element Method in Engineering Science, London: McGraw-Hill.